Mon. Not. R. Astron. Soc. **000**, 000–000 (0000) Printed 12 September 2014 (MN LATEX style file v2.2)

Subhaloes gone Notts: Subhaloes as tracers of the dark matter halo shape

Kai Hoffmann⋆[1], Susana Planelles[2,3], Enrique Gaztañaga[1], Alexander Knebe[4], Frazer R. Pearce[5], Hanni Lux[5,6], Julian Onions[5], Stuart I. Muldrew[5], Pascal Elahi[7,8], Peter Behroozi[9], Yago Ascasibar[4], Jiaxin Han[7,10], Michal Maciejewski[11], Manuel E. Merchan[12], Mark Neyrinck[13], Andrés N. Ruiz[12], Mario A. Sgro[12]

[1] *Institut de Ciències de l'Espai (ICE, IEEC/CSIC), E-08193 Bellaterra (Barcelona), Spain*
[2] *Astronomy Unit, Department of Physics, University of Trieste, via Tiepolo 11, I-34131 Trieste, Italy*
[3] *INAF, Osservatorio Astronomico di Trieste, via Tiepolo 11, I-34131 Trieste, Italy*
[4] *Departamento de Física Teórica, Módulo 15, Facultad de Ciencias, Universidad Autónoma de Madrid, 28049 Madrid, Spain*
[5] *School of Physics & Astronomy, University of Nottingham, Nottingham, NG7 2RD, UK*
[6] *Department of Physics, University of Oxford, Denys Wilkinson Building, Keble Road, Oxford, OX1 3RH, UK*
[7] *Key Laboratory for Research in Galaxies and Cosmology, Shanghai Astronomical Observatory, Shanghai 200030, China*
[8] *Institute for Astronomy, The University of Sydney, NSW 2006, Australia*
[9] *Space Telescope Science Institute, Baltimore, MD 21218, USA*
[10] *Institute for Computational Cosmology, Department of Physics, Durham University, South Road, Durham DH1 3LE, UK*
[11] *Max-Planck-Institut für Astrophysik, Garching, Karl-Schwarzschild-Strae 1, 85741 Garching bei Muenchen, Germany*
[12] *Instituto de Astronomía Teórica y Experimental (CCT Cordoba, CONICET, UNC), Laprida 922, X5000BGT, Cordoba, Argentina*
[13] *Department of Physics and Astronomy, The Johns Hopkins University, 3400 N. Charles St., Baltimore, MD 21218, USA*

arXiv:1401.2060v2 [astro-ph.CO] 10 Sep 2014

Received date / Accepted date

ABSTRACT

We study the shapes of subhalo distributions from four dark-matter-only simulations of Milky Way type haloes. Comparing the shapes derived from the subhalo distributions at high resolution to those of the underlying dark matter fields we find the former to be more triaxial if the analysis is restricted to massive subhaloes. For three of the four analysed haloes the increased triaxiality of the distributions of massive subhaloes can be explained by a systematic effect caused by the low number of objects. Subhaloes of the fourth halo show indications for anisotropic accretion via their strong triaxial distribution and orbit alignment with respect to the dark matter field. These results are independent of the employed subhalo finder. Comparing the shape of the observed Milky Way satellite distribution to those of high-resolution subhalo samples from simulations, we find an agreement for samples of bright satellites, but significant deviations if faint satellites are included in the analysis. These deviations might result from observational incompleteness.

Key words: methods: numerical - galaxies: haloes - cosmology: miscellaneous

1 INTRODUCTION

The modelling of how galaxies trace the underlying matter field is one of the biggest uncertainties in observational cosmology. Understanding the relation between the distributions of galaxies and matter at small scales, such as those of galaxy groups and clusters, turns out to be difficult due to the non-linear evolution of matter density fluctuations and the complex processes involved in galaxy formation. However, it is worth addressing this challenge as modelling the galaxy distribution at these scales increases the statistical power of cosmological surveys. Furthermore, it opens the possibility to compare model predictions to the well observed properties of our local Universe.

The host haloes of galaxy groups and clusters can be characterised by their radial density profiles and their triaxiality. In this study we are interested in the latter property as we analyse the relation between the shape of dark matter haloes obtained from high resolution simulations and their subhalo populations. The relation between these shapes is

⋆ E-mail: hoffmann@ice.cat

relevant for the Halo Occupation Distribution models, which are used to predict and interpret observational data. In these models, satellite galaxies are distributed in host haloes with an assumed ellipticity. This ellipticity has an impact on the correlation functions derived from these models (e.g. Smith and Watts 2005; Smith et al. 2006; van Daalen et al. 2012).

Observations of the local Universe suggest that the shapes of host haloes and those of their satellite populations are not necessarily the same since the satellites are found to be distributed along thin discs. During recent years, the discs of satellite galaxies around the Milky Way (MW; Lynden-Bell 1976; Demers and Kunkel 1976) and the Andromeda galaxies (M31; Koch and Grebel 2006; Metz et al. 2007, 2009; Pawlowski et al. 2012; Conn et al. 2013) are discussed in the literature with focus on whether or not such flat satellite distributions around MW-like host haloes are expected in the standard, spatially flat Λ-*Cold Dark Matter* model with cosmological constant (ΛCDM, Blumenthal et al. 1984).

Within this hierarchical model of structure formation, haloes accrete matter from preferential directions of the surrounding sheets and filaments. As a consequence, the substructure distribution in haloes is not expected to be spherical until the orbits of the accreted matter components are completely randomized (Knebe et al. 2004; Zentner et al. 2005; Libeskind et al. 2005). Such an anisotropic accretion of substructures was first observed in simulations by Tormen (1997) (see Vera-Ciro et al. 2011; Lovell et al. 2011; Libeskind et al. 2012, for recent studies). Indeed, flat satellite systems are also found in CDM N-body simulations, albeit those are unlikely to be as flat as the satellite systems of the MW and M31 (see e.g. Wang et al. 2013, who also take into account possible obscuration effects from the galactic disc). However, ΛCDM simulations of the local Universe with constrained initial conditions are able to reproduce the galaxy distributions in our neighbourhood. Analysing a set of such simulations, Libeskind et al. (2011) found that the local satellite distribution probably results from anisotropic accretion of matter.

Light was shed from a different angle on the anisotropic accretion scenario by Danovich et al. (2012). Simulating dark matter together with gas in hydrodynamical simulations these authors find that, at high redshifts, a large fraction of the baryonic mass of massive haloes is accreted from a few narrow streams of cold gas which tend to lie in the same sheets of the dark matter distribution. This effect leads to thin discs of satellites (Goerdt and Burkert 2013) and might explain why planar subhalo distributions as thin as the MW and M31 are unlikely to be found in DM–only simulations.

However, discrepancies between the discs of satellites in ΛCDM simulations and observations of the local group as well as the missing satellite problem (e.g. Weinmann et al. 2006) motivate the exploration of alternative formation scenarios, within which the discs of satellites could originate from tidal arms developed during an encounter of a young MW with another galaxy (e.g. Pawlowski et al. 2012, suggested M31 for the large magellanic cloud). Such events are observed (e.g. Weilbacher et al. 2003) and can be also seen in simulations (e.g. Bournaud et al. 2008) without requiring the assumption of cold dark matter.

In this study we aim to improve the understanding of why massive subhaloes in ΛCDM simulations are distributed anisotropically around the centre of their host halo. We therefore examine the shape of the dark matter subhalo populations in four MW-like host haloes from the Aquarius simulation to disentangle systematic effects from anisotropic accretion as possible explanation for the flat distribution of the most massive subhaloes. Two possible systematics are studied:

i) Substructures in dark matter haloes are not well defined objects. After accretion, dark matter particles can move away from the subhalo, as the latter orbits under the action of the complex gravitational field of its host. The question if a given dark matter particle is still associated to the subhalo within which it entered the host can be answered differently by different subhalo finders. The resulting uncertainty of subhalo properties (e.g. mass) causes the problem that subhalo samples, defined by these properties, can consist of different objects, depending on the employed subhalo finder. Uncertainties of subhalo properties can therefore propagate into uncertainties in the shape of their distribution if, for instance, the N most massive subhaloes are analised.

ii) Besides the detection of subhaloes in simulations, the small number of massive (observationally speaking, the most luminous) subhaloes complicates the shape measurement of their distribution. Ensembles with low numbers of objects are more likely to appear aligned, which can cause an apparent, non-physical flattening of subhalo distributions.

Looking for indications of anisotropic infall, we also investigate the orbit orientation of subhaloes, given by the direction of their angular momenta, with respect to the dark matter field of the corresponding host haloes.

Finally, after investigating possible reasons for the flatness of the Aquarius subhalo populations, we compare the shape of these populations to results computed from the observed MW satellite distribution.

This paper is organised as follows: in Section 2 we describe the simulations analysed in this work together with the different subhalo finders participating in this study; in Section 3 we introduce the method used to derive halo shapes. Shape measurements of haloes and their subhalo population are presented in Section 4 together with an analysis on subhalo orbit orientation with respect to the dark matter field and a comparison with shapes of the observed MW satellite distribution. Finally, our findings are summarised and discussed in Section 5. In the Appendix, we study the accuracy and precision of our shape measurements and present the observational data.

2 SIMULATIONS

We study subhalo populations from four simulated Milky Way sized host haloes. These haloes are part of the Aquarius simulation project (Springel et al. 2008) - a suite of high resolution N-body simulations performed using the cosmological SPH code GADGET-3 (based on GADGET-2, Springel 2005). The simulated haloes were selected from the larger cosmological ΛCDM simulation Millennium-II (Boylan-Kolchin et al. 2009) and then re-simulated at higher resolution with the cosmological parameters $\Omega_m = 0.25$,

Halo	particle mass $[h^{-1}\mathrm{M}_\odot]$
Aq-A-2	1.877×10^4
Aq-A-4	5.382×10^5
Aq-B-2	8.832×10^3
Aq-B-4	3.071×10^5
Aq-C-2	1.916×10^4
Aq-C-4	4.401×10^5
Aq-D-2	1.914×10^4
Aq-D-4	3.667×10^5

Table 1. Haloes from the Aquarius simulation analysed in this work. The left column shows the simulation name, encoding the halo (A to D), and the resolution level (2 and 4); the corresponding particle masses are shown in the right column, where $h = 0.73$.

$\Omega_\Lambda = 0.75$, $\sigma_8 = 0.9$, $n_s = 1$ and $H_0 = 100h$ km s^{-1}Mpc^{-1} $= 73$ km s^{-1}Mpc^{-1}.

The four Aquarius haloes analysed in this work, labeled from `Aq-A` to `Aq-D`, have final masses of $\sim 10^{12}\mathrm{M}_\odot$ and were chosen to be relatively isolated at redshift $z = 0$. Each halo has been re–simulated at five resolution levels, labeled as 5, for the lowest, to 1, for the highest resolution level, respectively. The mass per particle varies from $m_p = 2.94 \times 10^6 h^{-1}\mathrm{M}_\odot$ in level 5 to $m_p = 1.25 \times 10^3 h^{-1}\mathrm{M}_\odot$ in the highest resolution run, resolving a given halo with approximately half-million up to 1.5-billion particles within the virial radius for level 5 and 1, respectively. In our analysis we focus on subhaloes detected at the second highest level of resolution 2 at $z = 0$. Those are compared to the dark matter field at the second lowest level of resolution 4 (dark matter data from higher resolution runs was not available for this analysis). The particle masses of these haloes are shown in Table 1. More information on the haloes is given by Springel et al. (2008).

2.1 Subhalo Finders

Several subhalo finders have been applied on the Aquarius haloes. Each of them delivers a different subhalo catalogue, due to their specific numerical techniques. In order to minimize differences when comparing subhalo samples from different finders, a common post-processing pipeline has been applied. A detailed analysis of these subhalo catalogues can be found in Onions et al. (2012), whereas additional studies of the same data have been published in several recent papers resulting from the "Subhalo Finder Comparison Project" (e.g. Onions et al. 2013; Knebe et al. 2013; Elahi et al. 2013; Pujol et al. 2013).

Eleven subhalo finders participated in the comparison project. However, we present only results for the Amiga Halo Finder (AHF; Knollmann and Knebe 2009), SUBFIND (Springel et al. 2001), ROCKSTAR (Behroozi et al. 2013), and the STructure Finder (STF, also known as VELOCIraptor; Elahi et al. 2011), since only those where run at high resolution on all four Aquarius haloes, analysed in this work, due to their computational efficiency. For further details of the different halo-finding algorithms, we refer the reader to the corresponding code papers.

3 SHAPE MEASUREMENT

To quantify the shape of dark matter haloes and their subhalo populations we aim to approximate their isodensity contours with ellipsoids. This allows us to quantify shapes in terms of the axis ratios $q = b/a$ and $s = c/a$, where a, b and c are the major, intermediate and minor axis of the ellipsoid respectively. In the following we will refer to these axis ratios as shape parameters. Several methods have been introduced in the literature to approximate isodensity contours with ellipsoids, while most of them deliver similar results (see Allgood et al. 2006; Vera-Ciro et al. 2011). To evaluate the shape parameters we follow Dubinski and Carlberg (1991), by calculating the eigenvalues of the reduced moment of inertia

$$I_{i,j} = \sum_n^N \frac{r_{i,n} r_{j,n}}{r_{1,n}^2 + r_{2,n}^2 + r_{3,n}^2}, \qquad (1)$$

where $\mathbf{r_n} = (r_{1,n}, r_{2,n}, r_{3,n})$ is the position of the n^{th} object with respect to the halo centre and N is the number of objects (either dark matter particles or subhaloes) that fulfill $|\mathbf{r_n}| \leqslant 250\ h^{-1} kpc$. This radius was chosen to enclose all MW satellites, while it is larger than r_{200} of the considered Aquarius haloes, given by Springel et al. (2008). We chose the reduced instead of the usual moment of inertia to prevent objects with large distances to the halo centre from dominating the measurements.

The subhalo masses are set to unity to be unaffected by uncertainties in their determination and to simplify the comparison with observations. Assuming ellipsoidal distributions, the square root of the largest, intermediate and smallest eigenvalue corresponds to the absolute value of the major, intermediate and minor axis respectively, that is, $(a, b, c) = \sqrt{(\lambda_1, \lambda_2, \lambda_3)}$, with $\lambda_3 \leqslant \lambda_2 \leqslant \lambda_1$.

Contrary to what is often done, we do not measure shapes iteratively. In the iterative shape measurement particles that reside within the fitted ellipsoid are used to remeasure the shape, while for the initial measurement all particles are taken into account. This procedure is repeated until the shape parameters converge. We do not employ this method because during the iteration objects are excluded from the analysis which complicates the interpretation of shape measurements of, for instance, the N most massive subhaloes. Furthermore we found that q and s sometimes converge to zero during the iteration, when only a few particles are analysed. Bailin and Steinmetz (2005) showed that, if shape measurement is performed without iteration, selecting particles in a sphere biases the measured shape parameters towards spherical results. We have verified these results using the `Aq-A` dark matter field. However, in this study we are not interested in the exact values of the shape parameters, but more in how the shapes of the subhalo populations are related to those of their hosts.

Besides the method for deriving the axis ratios, shape measurements can depend on the definition of the halo centre. A possible offset between the centre of mass of the host halo and the one of the full matter distribution, caused by massive substructure, can introduce an artificial triaxiality, especially when shapes are measured within the central part of a halo. Moreover, an offset can indicate an unrelaxed condition of the halo according to results of Power et al. (2012), who found that the distance between the most bound par-

ticle and the centre of mass is correlated with the virial ratio of the halo. To find the centre of the host halo we apply the following procedure: i) particles within the distance R/n around the centre of mass are selected to recalculate a new centre of mass, where n is initially set to unity and R is the largest particle distance to the centre of mass at the highest resolution level. ii) Step i) is repeated $n = 100$ times, while n is increased by one in every iteration step. Visual inspection confirmed that the centre determined by this procedure corresponds to the centre of the host halo. We use the host halo centre for the shape measurement of both - the dark matter field, as well as the subhalo population. This approach is chosen because it is easily applicable to observational data sets, assuming that the most luminous galaxy (e.g. the MW) resides in the centre of the host halo (see e.g. Vale and Ostriker 2004). This latter assumption might be wrong in some cases (see e.g. Skibba et al. 2011; Trujillo-Gomez et al. 2011).

4 RESULTS

In this section we present our shape measurements of the Aquarius subhalo populations and compare them to the shape of the underlying dark matter field as well as to observational data.

In the whole analysis we quantify subhalo masses with the values of the current maximum rotational velocity $v_{\rm max}$ with which dark matter particles orbit around the subhalo centre. Kravtsov et al. (2004) found that these $v_{\rm max}$ values are correlated with the subhalo masses, even during tidal stripping. Onions et al. (2012) demonstrated that when $v_{\rm max}$ is used as mass proxy the mass function of subhaloes obtained from different halo finders are in better agreement with each other than for M_{200}. This might be explained by $v_{\rm max}$ measurements being less dependent on uncertain definitions, such as the subhalo boundaries.

4.1 Distribution of subhalo populations identified by different finders

To gain a visual impression of how subhaloes are distributed around the centre of their host halo we display the `Aq-A` dark matter field together with its subhalo population in Figure 1. The halo is rotated so that the intermediate axis of the ellipsoid approximating the dark matter isodensity contours stands perpendicular to the plane of the figure. This ellipsoid is fitted to the dark matter distribution within a 250 $h^{-1}kpc$ sphere around the halo centre. The coloured area denotes the normalised projected density of the dark matter particles at the second lowest level of resolution (level 4) within a 100 $h^{-1}kpc$ slice through the halo centre and parallel to the intermediate axis. The full dark matter field at different resolution levels was not available for our analysis, whereas we do not expect this limitation to affect our conclusions as discussed in Section 4.2. The black-rimmed green dots denote the positions of the 13 and 50 highest $v_{\rm max}$ subhaloes [1] (top and bottom panels, respectively), identified by the subhalo finders AHF, SUBFIND, ROCKSTAR and STF at the second highest level of resolution (level 2).

We find that the subhalo distributions identified by the different halo finders differ only by a few objects. Especially the results of AHF and SUBFIND agree very well with each other. We also find that the 13 `Aq-A` subhaloes with the highest $v_{\rm max}$ values are roughly aligned with the major axis of the dark matter field, while their distribution is flatter. An alignment in the same direction is also apparent for the 50 subhaloes with the highest $v_{\rm max}$ values, while the shape of their distribution is more isotropic and, therefore, in better agreement with the shape of the underlying dark matter field.

A physical explanation for the flattening of the massive subhalo population might be that massive objects maintain information about their infall direction for a longer time due to their large moment of inertia, while the orbits of low mass subhaloes randomise faster after infall. If subhaloes are accreted anisotropically, the triaxiality of a given subhalo distribution might therefore increase the more massive objects are contained in the samples. Furthermore tidal forces can strip of material from subhaloes, while they orbit around the centre of their host. This might introduce an additional correlation between the subhalo mass and its orbit orientation with respect to the infall direction. Another reason might be that dynamical friction causes massive subhaloes to sink faster to the host center. For this reason they might more prone to be totaly disrupted before developing circular orbits, as suggested by Gill et al. (2004). However, due to the small number of massive subhaloes the flatness of their distribution might be an effect of random sampling. We attempt to disentangle such a systematic effect from anisotropic accretion as reasons for the flatness in Section 4.2.

4.2 Flatness of the subhalo population

Focusing the analysis on the flattening of the massive subhalo population with respect to the dark matter field we measure their shapes using results from the four haloes `Aq-(A-D)`. To quantify shapes we follow the procedure described in Section 3 by determining the largest, intermediate and smallest eigenvalues of the reduced moment of inertia (a, b, c respectively). The latter is constructed from objects (either dark matter particles or subhaloes) that reside within a 250 $h^{-1}kpc$ sphere around the halo centre. The shape can then be quantified by the shape parameters $q = b/a$ and $s = c/a$ which correspond to the axis ratios of ellipsoids approximating the dark matter and subhalo distributions. Note that according to this definition, the extreme cases $q = s = 1$, $s \ll q = 1$ and $q = a \ll 1$ correspond, respectively, to a sphere, a disc and a filament.

[1] The selection of the 13 highest $v_{\rm max}$ subhaloes is motivated by the set of 13 MW satellites that are brighter than $M_V = -8.5$, listed in Table C1. This set of satellites consists mostly of objects detected before the SDSS analysis (the "classical" satellites). The number of highest $v_{\rm max}$ subhaloes in the larger sample corresponds to the 50 MW satellites, predicted by Simon and Geha (2007) for a completely observed sky.

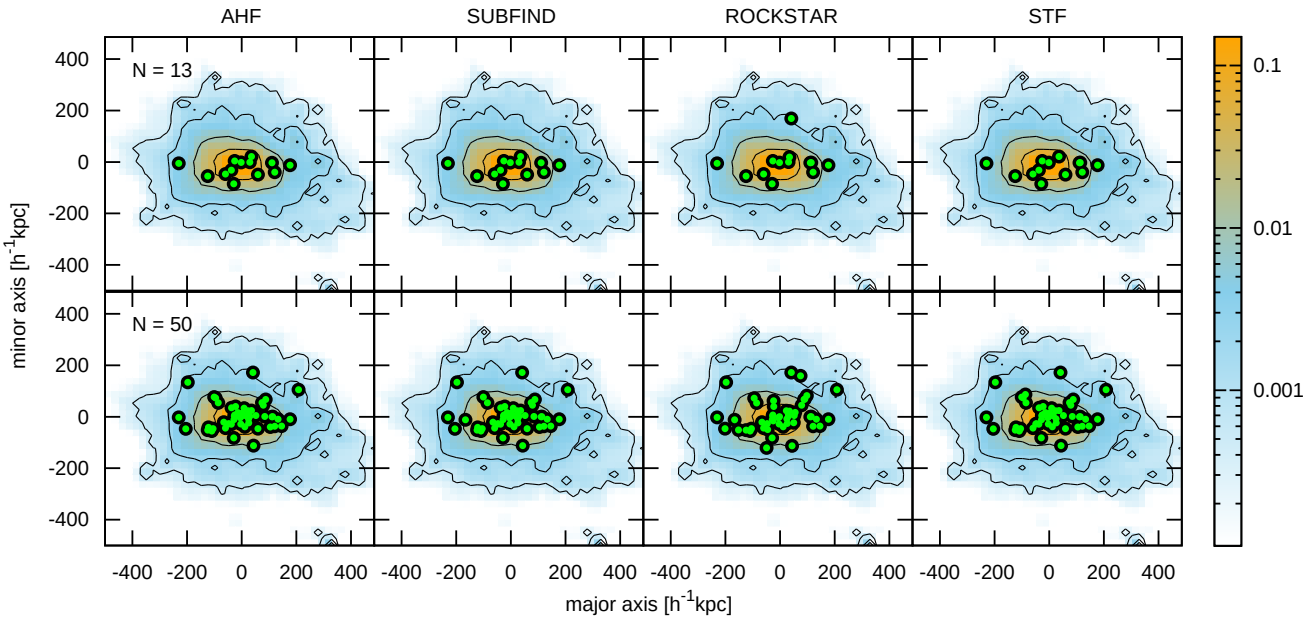

Figure 1. Matter distribution of the `Aq-A` halo together with the population of the 13 (upper panels) and the 50 (bottom panels) subhaloes with the highest $v_{\rm max}$ values. Colours shown on the right bar denote the normalised density of dark matter at the resolution level 4 in a 100 $h^{-1}kpc$ slice through the halo centre perpendicular to the intermediate axis measured at 250 $h^{-1}kpc$. The black-rimmed green dots denote positions of the N `Aq-A` subhaloes with highest $v_{\rm max}$ values within a sphere of 250 $h^{-1}kpc$ identified by the subhalo finders AHF, SUBFIND, ROCKSTAR and STF at resolution level 2. Note that in the case of ROCKSTAR and STF only 12 of the 13 highest subhaloes are visible since one is obscured by other subhaloes.

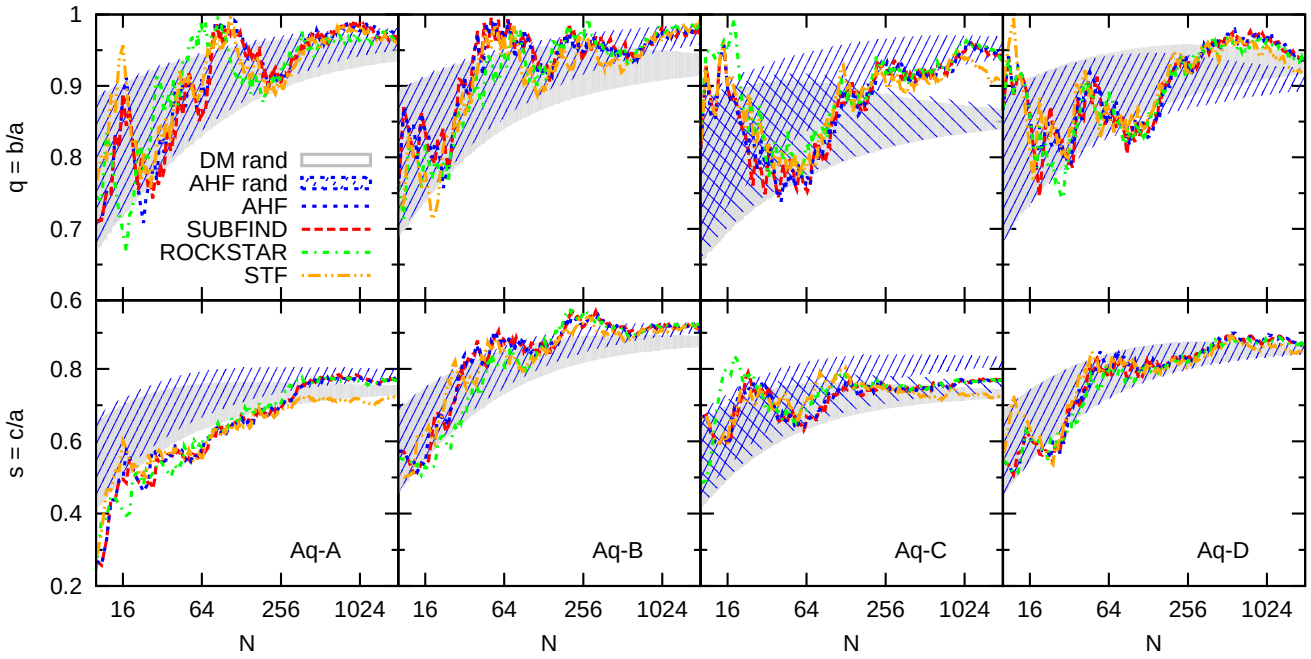

Figure 2. Shape parameters q (upper panels) and s (bottom panels) of `Aq-(A-D)` subhalo populations (panels from left to right) at the resolution level 2 for the N subhaloes with the highest $v_{\rm max}$ values within 250 $h^{-1}kpc$ around the halo centre. The blue hatched (grey) areas result from random selections of N subhaloes (dark matter particles at the resolution level 4) regardless of their mass. They denote 68% confidence levels derived from 1000 realisations of such random selections. As explained in Subsection 4.2.1, the wide blue hatched area in the panel for the `Aq-C` halo results from a validation test to explain the difference between shapes from dark matter and subhalo random samples.

4.2.1 Systematic bias in shape measurements from small numbers of tracers

A systematic bias in the shape measurement towards triaxiality from low numbers of shape tracing points (in our case subhaloes) is expected since any discreteness noise will produce a nonzero ellipticity even from a perfectly spherical object. In the extreme cases of two and three tracer points any density field will be classified as a filament and disc respectively. This known effect (e.g. Paz et al. 2006; van Daalen et al. 2012; Joachimi et al. 2013) might be the reason why we measure smaller values of the shape parameters q and s for the distribution of the most massive subhaloes than for larger sets including less massive subhaloes or the dark matter field.

We show in Fig. 2 the values of q and s measured from the distributions of the N most massive `Aq-(A-D)` subhaloes using $v_{\rm max}$ as a proxy for mass. Different coloured line types stand for the results of the subhalo samples obtained from the four halo finders that were run at the resolution level 2 on all haloes. The shape parameters show a $\Delta q \simeq \Delta s \simeq 0.1$ scatter when roughly more than 100 subhaloes are used for the measurement. For smaller numbers of subhaloes results from different finders show a stronger scatter of around $\Delta q \simeq \Delta s \simeq 0.2$. A more detailed analysis based on results from ten subhalo finders, run at all five resolution levels of the `Aq-A` halo, revealed a stronger scatter for a larger variety of finders, which tends to increase at low resolution. At the lowest resolution level 5 we find a scatter of roughly $\Delta q \simeq \Delta s \simeq 0.4$ for samples consisting of the 13 highest $v_{\rm max}$ subhaloes, partly because of the larger number of finders run at low resolution. This finding suggests that the shapes of subhalo populations consisting of the highest $v_{\rm max}$ objects in MW-like host haloes, measured in currently high resolution cosmological simulations, strongly depend on the subhalo finder employed to identify substructures.

As indicated by the visual impression from Fig. 1 the shape parameters increase (shapes become more spherical) if more subhaloes with lower mass (lower $v_{\rm max}$ values) are used for the shape measurement. This effect is apparent for all four haloes `Aq-(A-D)`, while the measurements also show strong fluctuations for different numbers of most massive subhaloes. We mentioned Section 4.1 that the decrease of shape parameters for the N most massive subhaloes might be caused by physical effects, such as anisotropic infall, but also by a systematic effect resulting from small numbers of subhaloes in these samples.

To distinguish between the two possible reasons for the flatness, we generate random samples of N AHF subhaloes that are randomly selected from all detected subhaloes within a given halo, independently of their $v_{\rm max}$ value. If the shape parameters of the distribution of the N most massive subhaloes are significantly smaller than the values obtained from many random samples, then this would indicate a physical reason for the flatness. Systematics from small numbers of subhaloes should not cause differences between shapes from the two types of samples, since both consist of the of the same number of objects. We generate 1000 random samples, each with N AHF subhaloes, from which we obtain median values of the shape parameters and 68% probability regions as indicator for the scatter. The latter is shown as a blue hatched region in Fig. 2. We find that the shape parameters q and s of the distributions of the N most massive subhaloes roughly lie within the central 68% region of q and s measurements derived from random samples. We have tested that randomly sampling subhaloes identified by different subhalo finders leads to the same result. In most cases, the increased triaxiality (smaller shape parameters) of the N most massive subhaloes with respect to the dark matter field can therefore be explained by a systematic bias in the shape measurement due to small numbers of objects. An exception of this result is the s parameter of `Aq-A`, which is significantly smaller for samples of the N most massive subhaloes than the expected value from random sampling. We will discuss this finding in Section 4.2.2 in more detail.

The results in Fig. 2 also show that the variation between shape measurements for subhalo populations at level 2 from different finders is smaller than the noise in the measurement, expected from random sampling. The aforementioned scatter at low resolution is comparable to the noise from random sampling.

When the number of considered shape tracers is above 1000 the shape measurements start to converge to certain values of q and s. Studying the shapes of artificial haloes we find that the convergence of the shape parameters for large numbers of tracer particles depends on the halo shape. The number of particles necessary to reach a certain precision in the shape measurement increases the closer a halo is to spherical symmetry, while in that case roughly 1000 tracer particles are needed for a 10% precision (see Fig. A1 in Appendix A). Note that this result might depend on the exact method used for the shape measurement. Although similar results are reported by authors using different definitions of the moment of inertia (e.g. Joachimi et al. 2013), further study might be worthwhile to explore how heavily different shape measurements are affected by discreteness noise.

Comparing the shapes of the distributions of the N most massive subhaloes with the dark matter halo shape, taking into account the bias in the measurements from low numbers of objects, we also generate 1000 samples of N randomly selected dark matter particles from each Aquarius halo at the resolution level 4, instead of using subhaloes. As mentioned before, only the resolution level 4 was available for this analysis. Vera-Ciro et al. (2011) demonstrated that their `Aq-A` dark matter halo shape parameters at the five resolution levels differ by less than 4% from each other, when the measurement is performed at radii as large as those used in our study (250 $h^{-1}kpc$). Their shape parameters measured from dark matter particles within 250 $h^{-1}kpc$ around the halo centre are smaller than ours, in part because we measure shapes without iteration. We are able to roughly reproduce their results if we measure the dark matter shapes iteratively as well. Moreover, the difference between our measurement of the shape parameter s derived with and without iteration is consistent with results reported by Bailin and Steinmetz (2005).

Besides measuring dark matter shapes without iteration a further difference to the measurements of Vera-Ciro et al. (2011) is that we do not exclude particles that are members of subhaloes from the analysis. We do not follow this approach, as the relation between the shape of the subhalo population and the full dark matter shape is closer to observational information, as dark matter halo shapes might be traced for example by X-ray or lensing signals, which result

from the full mass distribution. The 68% probability regions of the 1000 shape measurements are shown as grey regions in the same figure.

If the random samples of subhaloes and dark matter particles consist only of a few objects, both types of random samples show similar distributions of the shape parameters. However, for larger numbers of objects, the shape parameters of subhalo and dark matter random samples do not converge to the same values. We can explain this result if we bear in mind that each substructure is represented by just one single object (the subhalo) in case of the subhalo random samples, but as several objects (the dark matter particles of the subhalo) in case of the dark matter random samples. This feature might introduce an artificial anisotropy in the dark matter moment of inertia which is reflected by smaller shape parameters. In this sense, the fact that the difference between shape measurements from random subhalo and dark matter particle samples is stronger for the `Aq-C` halo might be related to the fact that this halo has more high-mass substructures, as it can be seen in Fig. 3 from Springel et al. (2008).

To gain a better understanding of this effect, we perform a simple test that consists in giving more weight to the massive subhaloes during the random selection. For this purpose, we simply write subhaloes with large values of $v_{\rm max}$ ($v_{\rm max} > 100\,km/s$) 2000 times in the subhalo catalogue and repeat the shape measurement from random samples. Following this simple approach, we can roughly reproduce the results from the dark matter random sampling, as shown by the additional wide blue hatched area included in the panel for the `Aq-C` halo in Fig. 2. For the sake of clarity, we only show the result of this test for the `Aq-C` halo, although we have checked that we obtain similar results for the rest of Aquarius haloes.

This same effect could have been tested by excluding dark matter particles in subhaloes from the measurement.

4.2.2 Anisotropic infall

We found in the previous section that the value of s measured from the N most massive `Aq-A` subhaloes is significantly below the expected value from randomly sampling subhaloes (Fig. 2). It is therefore unlikely that the flatness of the `Aq-A` population of massive subhaloes can be explained by random sampling. Since this effect is independent of the employed subhalo finder we show, for the sake of clarity, here and in the following analysis only results derived from AHF subhalo populations. We have tested that our conclusions do not change when employing different finders.

Focusing the analysis on the flatness of the massive `Aq-A` subhaloes we show in the top panel of Fig. 3 the significance of the deviation between the shape parameter s of the N most massive `Aq-(A-D)` subhaloes and the median values obtained from randomly sampling subhaloes. We define this significance as the ratio of the deviation and the error obtained from randomly sampling subhaloes, shown as blue hatched areas in Fig. 2. Again, we see that the `Aq-A` subhalo population is significantly flatter than expected from random sampling, while the flatness of massive subhalo populations in the other haloes lies within the expected range.

In order to understand this particular result, we study, in the following, anisotropic infall as an additional source of flattening. A proper way to study anisotropic infall would be to follow the subhalo positions through different time steps of the simulation, like for example Libeskind et al. (2005). However, since this data is not available within the present comparison project, we investigate the orbit orientation of subhaloes given by the direction of their angular momenta with respect to the dark matter field of the corresponding host haloes. This approach is motivated by the following consideration: if the N highest $v_{\rm max}$ subhaloes do not accidentally lie in a plane, then also their orbits should lie within the same plane, possibly because they entered the host halo from a similar direction. The angular momentum $\mathbf{J}$ of this subhalo population should therefore be aligned with the minor axis of the ellipsoid fitted to the dark matter halo, if the orbital plane is contained within the plane defined by the major and intermediate axes of the dark matter ellipsoid (hereafter referred to as the major plane).

We calculate the total angular momentum of subhalo populations as

$$\mathbf{J} = \sum_{n}^{N} \mathbf{J_n}\,, \tag{2}$$

where $\mathbf{J_n} = \mathbf{r_n} \times \mathbf{v_n}$ is the angular momentum of the n^{th} subhalo, $\mathbf{r_n}$ and $\mathbf{v_n}$ are the corresponding position and velocity vectors with respect to the halo centre and its velocity, and N stands for the number of highest $v_{\rm max}$ subhaloes. As in the computation of the moment of inertia, all subhalo masses are set to unity.

In the bottom panel of Fig. 3 we show the angle between the minor axis of the dark matter field of each host halo `Aq-(A-D)` and the total angular momentum of the corresponding subhalo populations when we take samples consisting of the N highest $v_{\rm max}$ subhaloes. We find that this angle is smaller for `Aq-A` than for the other haloes, indicating a stronger alignment between the subhalo populations angular momentum and the dark matter minor axis. If we associate this stronger alignment with the effects of anisotropic infall, this result suggests that anisotropic infall can slightly increase the flattening of the subhalo populations, while the main reason for the flattening is the bias in the shape measurement due to small numbers of objects.

Note that the individual subhaloes do not contribute equally to the total angular momentum, since they are weighted by their distance and velocity with respect to the halo centre. Consequently, few objects with high velocities, large distances to the centre, or both can dominate the measurement. We therefore study in the following the flattening of subhalo populations and their rotational support with quantities that are defined for individual objects.

We start with a complementary method to study the degree of flattening of the subhalo population which consists in analysing the distribution of distances of the individual subhaloes to the major plane of the dark matter ellipsoid. From the subhalo distances to the dark matter major plane, d_c we derive the mean over the whole subhalo population, $d_{c,\rm mean}$. We show the mean relative distance $d_c/d_{c,\rm mean}$ as computed in bins of 11 subhaloes with the highest $v_{\rm max}$ values in the top panel of Fig. 4. For each bin we also show error bars that enclose the 68% of the values around the mean of the distribution. In general, we find that the subhaloes of `Aq-(B-D)` with the highest $v_{\rm max}$ values do not lie significantly closer

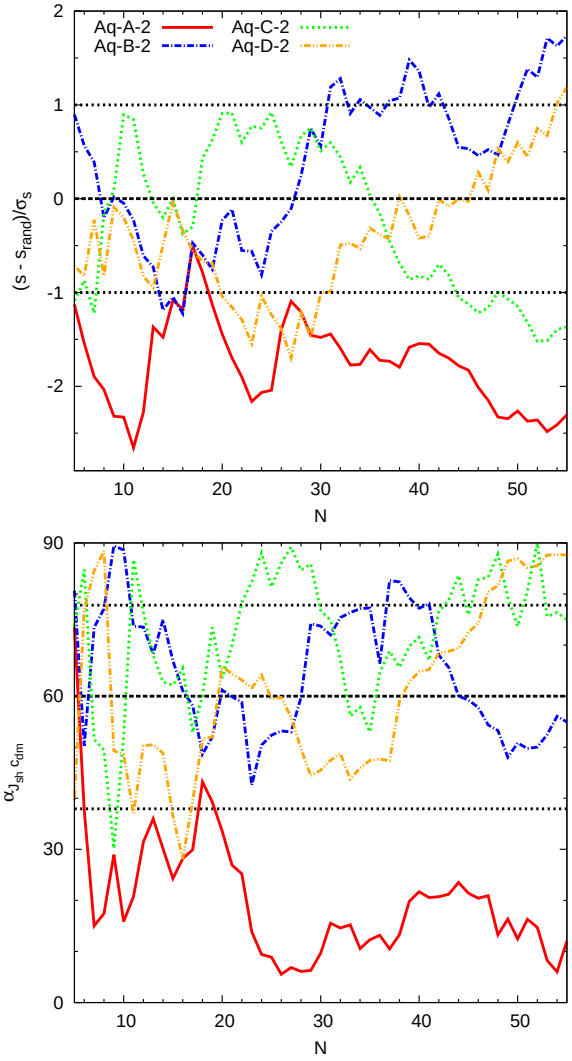

Figure 3. *Top panel:* Difference between the shape parameter s calculated from the N most highest $v_{\rm max}$ AHF subhaloes and the median value of 1000 shape measurements from N randomly selected AHF subhaloes ($s_{\rm rand}$) divided by the 1σ errors, shown as a hatched area in Fig. 2. *Bottom panel:* Angle between the total angular momentum of the subhalo population (with subhalo masses set to unity) and the minor axis of the dark matter field. The dashed and dotted lines indicate the mean angles $\pm 1\sigma$ deviations from an isotropic distribution respectively.

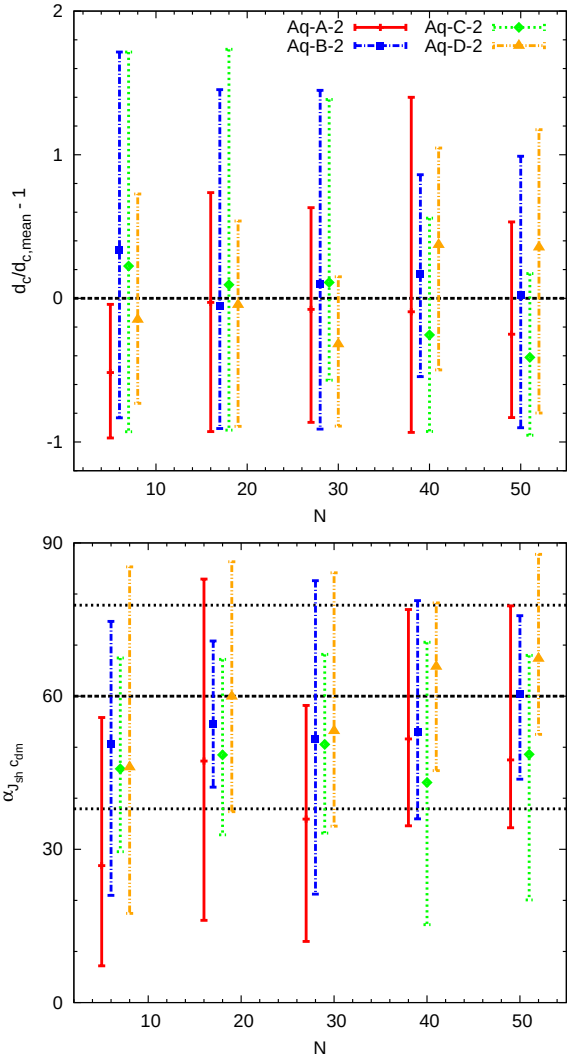

Figure 4. *Top panel:* Distance, d_c, of each subhalo to the plane spanned by the major and the intermediate axis of the dark matter moment of inertia in units relative to the mean distance to the same plane computed over the whole subhalo population. Symbols show the mean $d_c/d_{c,\rm mean} - 1$ over N $\pm$ 5 AHF subhaloes with the highest $v_{\rm max}$ values. Error bars enclose the central 68% of the distribution in each bin. *Bottom panel:* Angle between angular momentum of each subhalo and the minor axis of the dark matter moment of inertia. Binning and error bars are calculated in the same way as in the top panel. The dashed and dotted lines indicate the mean angles $\pm 1\sigma$ deviations from an isotropic distribution respectively.

to the major plane of the dark matter field than the mean over the whole population. The situation is slightly different for `Aq-A`, whose most massive subhaloes seem to be closer to the major plane, indicating therefore a flatter distribution. This result is consistent with those from shape measurements shown in Fig. 3, where we derived cumulative instead of differential values of subhalo populations with the highest $v_{\rm max}$ values.

In order to verify rotational support, we measure for each subhalo separately the angle between the angular momentum and the minor axis of the ellipsoid fitted to the dark matter field as $\alpha_n = \arccos(\hat{J}_n \cdot \hat{c}_{dm})$. Using the same bins of 11 subhaloes sorted by $v_{\rm max}$ as in the top panel of Fig. 4, we now show, in the bottom panel of the same figure, the mean values of α_n in each bin together with the the error bars which enclose the central 68% of the distribution. In agreement with our previous results, we find that the `Aq-A` subhalo population, which is significantly flattened, is also stronger aligned with the minor axis of the dark matter ellipsoid than it is the case for the other haloes. These findings point towards an scenario in which the flatness of the `Aq-A` subhalo population can be partially explained by the effects of anisotropic infall.

Results of Vera-Ciro et al. (2011) also support this scenario (see their Fig. 8). These authors show that material falling into the `Aq-A` halo has a strong dipole component between $11 - 8$ *Gyr* lookback time, indicating filamentary ac-

cretion. The dipole components that they find for the other haloes are smaller, as material was accreted more isotropically. This result also confirms the reports by Lovell et al. (2011) who also found indications for anisotropic accretion by studying the alignment between the angular momenta of Aquarius subhaloes (as detected by SUBFIND) and their dark matter host halo. More specifically, Lovell et al. (2011) found that the distribution of angular momentum directions of subhaloes with the 11 largest progenitors had the strongest dipolarity in the case of `Aq-A`.

4.3 Comparing shapes of simulated subhalo populations with those of MW satellites

In this Section we compare the shapes of the Aquarius subhalo populations to those of the MW satellite population consisting of up to 27 objects within 250 $h^{-1}kpc$ around the galactic centre. As we have ranked subhaloes by their $v_{\rm max}$ values, we now use V-band luminosities to rank the satellite galaxies. Our comparison with MW data is therefore based on the assumption that the satellite galaxies with the brightest V-band magnitudes (M_V) live in the subhaloes with highest $v_{\rm max}$ values. As we use $v_{\rm max}$ as a proxy for the total subhalo mass, M_V can be used to quantify the stellar mass of a satellite galaxy (Baraffe et al. 1998). A weak correlation between the stellar mass of satellite galaxies in MW like halos and their $v_{\rm max}$ values can be found in simulations (Brooks and Zolotov 2012; Zolotov et al. 2012; Rodríguez-Puebla et al. 2013; Reddick et al. 2013). On the contrary, Libeskind et al. (2005) found that the stellar masses of semi-analytical model satellites are not correlated with the corresponding total subhalo mass at $z = 0$, but with the total mass of the main progenitor, as suggested by (Conroy et al. 2006). However, their employed model does not include tidal stripping of the stellar mass component. Despite the existing uncertainties, we assume that $v_{\rm max}$ is a convenient property for comparing results of the most massive subhaloes to those derived from the observed most luminous MW satellites. Note that all masses are set to unity in the definition of the moment of inertia from which we measure the shapes. The positions and V-band luminosities of the 27 MW satellites, taken from McConnachie (2012), are shown in the Appendix C.

The shape parameters measured from satellite populations consisting of the N brightest objects are shown as black lines in the left panel of Fig. 5. We also show the shape measurements of the `Aq-(A-D)` subhalo populations, consisting of the N objects with highest $v_{\rm max}$ values. We find that the absolute values of the shape parameters q measured from the satellite populations are similar to the results from simulations for samples that consist of the roughly twelve or less most massive objects. When fainter satellites are included to the measurement we find a decrease of q while the Aquarius results remain roughly constant, resulting in lower values for q in observations than in simulations. The increase of the q from `Aq-(A-D)` with the number of objects, which we have seen for large numbers in Fig. 2, is not apparent when the analysis is restricted to the 27 highest $v_{\rm max}$ subhaloes. In the case of the s parameter we find that the observational values tend to be below the results from simulations except for samples of the highest mass `Aq-A` subhaloes. Our values of s for the population of the twelve most luminous satellites is in rough agreement with those reported by Starkenburg et al. (2013). The s measurements for the twelve highest $v_{\rm max}$ subhaloes roughly agree with results that these authors obtain from randomly sampling satellites with $M_V < -8.5$ from semi-analytic models of galaxy formation imposed on the Aquarius simulation.

The stronger discrepancies between the shape parameters from observed satellite and simulated subhalo populations for larger samples might be explained by an angular selection effect, which has a stronger impact on faint objects. We expect selection effects to be twofold. On the one hand, galactic obscuration prevents us from detecting objects that lie close to the galactic plane. On the other hand, the sky is observed with an inhomogeneous intensity, due to the limited area of surveys. Both types of selection effects should affect stronger faint, as opposed to bright, objects. To study the effect of angular selection on the shape measurement we follow the procedure described by Wang et al. (2013) by measuring the shapes of the highest $v_{\rm max}$ `Aq-(A-D)` subhalo population residing within a light cone with an opening angle of $\alpha = 180 - 2\alpha_{\rm obs}$, where $\alpha_{\rm obs}$ is the angle of obscuration with respect to the galactic plane. Assuming that the orientation of this synthetic galactic plane is arbitrary, we conduct 1000 shape measurements with randomly oriented galactic planes. Orienting the galactic plane randomly is motivated by reports on the weak alignment of observed blue late-type galaxies and disc galaxies from hydrodynamic simulations with their surrounding matter distribution at large scales (Zhang et al. 2013; Joachimi et al. 2013; Sales et al. 2012; Hahn et al. 2010). The mean results of these 1000 shape measurements are shown in the right panel of Fig. 5. We find that both q and s are decreased when galactic obscuration is taken into account. Using an obscuration angle of $\alpha_{\rm obs} = 25^\circ$ we find that, for the population of all 27 satellites, the observational results for the shape parameters agree with those from simulations. If the analysis is restricted to the 12 brightest satellites, the observed shape parameters are higher than those from simulations. This indicates that faint samples are stronger effected by obscuration, as we have initially guessed. However, angular selection effects are probably more complicated than in our model. The obscuration angle of $\alpha_{\rm obs} = 25^\circ$ is larger than commonly reported for the MW. In Fig. C1 we see that the majority of satellites resides outside of this zone. This might be explained by a smaller obscuration angle together with the angular limitation of the SDSS (both shown in Metz et al. 2009), which result in a larger effective obscuration angle.

The black dashed lines in Fig. 5 show the shape parameters of satellite populations measured with a method that decreases the bias in the shape measurement from low numbers of shape tracing objects. This method is described in Appendix A.

5 SUMMARY AND CONCLUSIONS

We have analysed four high resolution simulations of dark matter haloes with MW-like masses from the Aquarius project, `Aq-(A-D)`, + to measure the shapes of their subhalo populations and compared them to those of the underlying dark matter distributions. Throughout the analysis we used

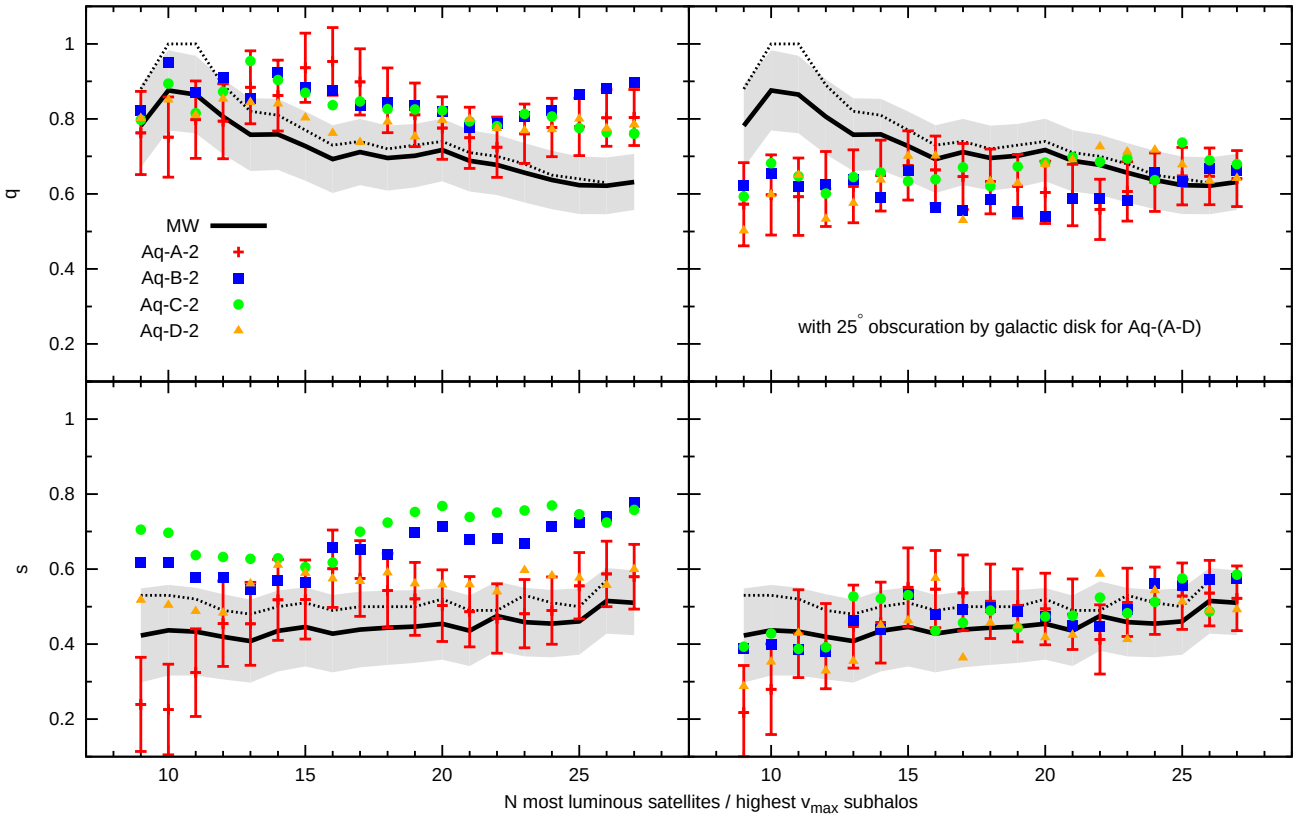

Figure 5. Shape parameters of the MW satellite distribution consisting in the N objects with highest V-band luminosities (black lines). These shapes are compared to those of Aquarius subhalo populations consisting in the N objects with highest $v_{\rm max}$ values identified by the AHF subhalo finder. The left panel shows results for the highest $v_{\rm max}$ subhaloes in the full sky. The right panel shows results for selecting subhaloes in a light cone with 130 degree opening angle, assuming 25 degree obscuration by the galactic disc. The coloured symbols denote the median values from 1000 realisations with randomly oriented light cones. The grey area and the error bars show the standard deviations estimated as described in the Appendix B. Black dashed lines show shape parameters from the MW data measured with a method that decreases systematic bias from low numbers of tracers, as described in Appendix A.

the $v_{\rm max}$ values of the subhaloes as a proxy for the subhalo mass.

We find that the shapes of subhalo populations, consisting of the objects with the highest $v_{\rm max}$ values show only a weak dependence on the employed subhalo finder when the subhaloes are analysed at high mass resolution. This result changes for small samples at lower mass resolutions since shape measurements for smaller subhalo samples are highly sensitive to changes of a few members. We therefore expect similar measurements, performed in currently high resolution cosmological simulations (e.g. Millennium-II), strongly depend on the subhalo finder used to identify substructures.

Our shapes measured from subhalo populations consisting of the N subhaloes with highest $v_{\rm max}$ values show that the subhalo distributions are more triaxial when only objects with highest $v_{\rm max}$ values are considered. This trend is apparent for all four halo finders run at the resolution level 2 and all four Aquarius haloes. Interpreting these results in terms of anisotropic accretion is delicate due to the fact that triaxiallity is likely to increase for samples with a few subhaloes. As a *null* test we conducted the same shape measurement for N randomly selected subhaloes and dark matter particles. In all cases we found a decrease of the shape parameters for small numbers of objects. In three of the four analysed haloes the decrease of the shape parameters for the subhaloes with highest $v_{\rm max}$ values is consistent with results from random samples. For `Aq-A` the shape parameter s is up to 40% smaller than the median value from random sampling. This difference roughly corresponds to a 2σ deviation and indicates a flattening of the population of high $v_{\rm max}$ subhaloes due to anisotropic infall.

To further verify if the flattening of the high $v_{\rm max}$ subhalo populations is not caused by random sampling, we studied the alignment of the angular momenta of the subhalo populations with the ellipsoid of the dark matter field. We found that the highest $v_{\rm max}$ `Aq-A` subhaloes are stronger aligned with the minor axis of the dark matter ellipsoid than the `Aq-(B-D)` subhalo populations. This finding indicates that the orbits of the high $v_{\rm max}$ `Aq-A` subhaloes tend to reside in the plane spanned by the major and intermediate axis of the dark matter moment of inertia, which is in agreement with subhalo accretion along the host halo major axis. Such an interpretation is consistent with the findings of Vera-Ciro et al. (2011), who showed that the matter accreted by the `Aq-A` halo has a dipole component - a signal of filamentary infall. Also Lovell et al. (2011) report indi-

cations for anisotropic accretion by studying the alignment between the angular momenta of Aquarius subhaloes and the dark matter field of their host halo.

After having analysed possible reasons for the increased triaxiallity of the highest $v_{\rm max}$ Aquarius subhaloes, we compare the shape of their distributions with those of observed MW satellites. In this regard, we found that the shape parameters derived for the distribution of the twelve satellites with the brightest V-band magnitudes lie within the range expected from the four Aquarius haloes when using the same number of subhaloes with the highest $v_{\rm max}$ values. However, for larger samples including fainter satellites and lower $v_{\rm max}$ subhaloes the shape parameters are below the results from simulations, especially the major to intermediate axis ratio q. This discrepancy can be decreased by assuming an overly strong galactic obscuration of 25°, while in that case the shape parameters for the high $v_{\rm max}$ samples lie below the results from bright satellites samples. This demonstrates that the geometry of our observational window, defined by the zone obscured by the galactic disc, and the geometry of the surveys mapping the sky can effect the shape measurements of the satellite distribution, while we expect a stronger impact on samples including faint satellites.

Within the ΛCDM context, the strong triaxiality of the MW satellite distribution with respect to our results from simulations can be interpreted as an result of anisotropic accretion, which would agree with the findings of Libeskind et al. (2011). A further reason for the strong flatness of the observed satellite distribution might be that the assumption that the most luminous satellites live in the subhaloes with the highest mass at redshift zero (using the maximum rotational velocity as mass proxy) might be inadequate to mimic the results of galaxy formation (Boylan-Kolchin et al. 2011). Simulations and observations suggest that the subhalo mass after infall and their stellar mass are not or just weakly correlated, while we assume a monotonic relation for our comparison with MW data (Libeskind et al. 2005; Brooks and Zolotov 2012; Rodríguez-Puebla et al. 2013). It might be necessary to simulate the evolution of dark matter together with the baryonic physics to produce thinner satellite discs (Danovich et al. 2012).

Our analysis of systematic effects on the shape measurement revealed that hundreds of tracers are needed for obtaining reliable results. We conclude that even if subhaloes, as potential hosts of satellite galaxies, follow the dark matter field of their host, they are to few for a reliable shape measurement of the MW dark matter halo. The expected increase of the number of known satellites in future surveys (Simon and Geha 2007) will probably not be sufficient to solve this problem. However, we also found that shapes of subhalo populations in three of four MW-like host haloes are consistent with the shapes of the dark matter field, if bias from the small number of tracers in the shape measurement is taken into account. The assumption that subhaloes trace the dark matter field of their host is therefore in reasonable agreement with our results.

A similar analysis performed on larger host haloes with more massive subhaloes at different redshifts would allow for an improved comparison with larger observational data sets from cosmological surveys.

ACKNOWLEDGEMENTS

This paper was initiated at the Subhaloes going Notts workshop in Dovedale, UK, which was funded by the European Commissions Framework Programme 7, through the Marie Curie Initial Training Network Cosmo- Comp (PITN-GA-2009-238356). We wish to thank the Virgo Consortium for allowing the use of the Aquarius dataset and Adrian Jenkins for assisting with the data.

KH is supported by beca FI from Generalitat de Catalunya. He acknowledges Noam Libeskind for a fruitful discussion. SP and HL acknowledge a fellowship from the European Commission's Framework Programme 7, through the Marie Curie Initial Training Network CosmoComp (PITN-GA-2009-238356). SP also acknowledges support by the PRIN-INAF09 project "Towards an Italian Network for Computational Cosmology" and by *Spanish Ministerio de Ciencia e Innovación* (MICINN) (grants AYA2010-21322-C03-02 and CONSOLIDER2007-00050). EG and KH acknowledge the *Spanish Ministerio de Ciencia e Innovación* (MICINN) project AYA2009-13936, Consolider-Ingenio CSD2007- 00060, AK is supported by the *Ministerio de Economía y Competitividad* (MINECO) in Spain through grant AYA2012-31101 as well as the Consolider-Ingenio 2010 Programme of the *Spanish Ministerio de Ciencia e Innovación* (MICINN) under grant MultiDark CSD2009-00064. He also acknowledges support from the *Australian Research Council* (ARC) grants DP130100117 and DP140100198. He further thanks Felt for penelope tree. SIM acknowledges the support of the STFC Studentship Enhancement Program (STEP). YA receives financial support from project AYA2010-21887-C04-03 from the former *Ministerio de Ciencia e Innovación* (MICINN, Spain), as well as the Ramón y Cajal programme (RyC-2011-09461), now managed by the *Ministerio de Economía y Competitividad* (fiercely cutting back on the Spanish scientific infrastructure). PSB is supported by a Giacconi Fellowship through the Space Telescope Science Institute, which is supported through NASA contract NAS5-26555. MN thanks the Sir John Templeton Foundation for support through a New Frontiers and Astronomy and Cosmology grant.

The authors contributed in the following ways to this paper: KH and SP undertook this project. KH performed the analysis presented and wrote the paper together with SP. KH is a PhD student supervised by EG. FRP, AK, EG, HL, JO and SIM contributed with useful discussions and with the organisation of the workshop at which this study was initiated. They designed the comparison study and planned and organised the data. The other authors provided data and had the opportunity to proof, read and comment on the paper.

REFERENCES

Allgood B., Flores R.A., Primack J.R., Kravtsov A.V., Wechsler R.H., Faltenbacher A., Bullock J.S., 2006, MNRAS, 367, 1781

Bailin J., Steinmetz M., 2005, ApJ, 627, 647

Baraffe I., Chabrier G., Allard F., Hauschildt P.H., 1998, A&A, 337, 403

Behroozi P.S., Wechsler R.H., Wu H.Y., 2013, ApJ, 762, 109

Blumenthal G.R., Faber S.M., Primack J.R., Rees M.J., 1984, Nature, 311, 517
Bournaud F., Duc P.A., Emsellem E., 2008, MNRAS, 389, L8
Boylan-Kolchin M., Springel V., White S.D.M., Jenkins A., Lemson G., 2009, MNRAS, 398, 1150
Boylan-Kolchin M., Bullock J.S., Kaplinghat M., 2011, MNRAS, 415, L40
Brooks A.M., Zolotov A., 2012, ArXiv e-prints
Conn A.R., et al., 2013, ApJ, 766, 120
Conroy C., Wechsler R.H., Kravtsov A.V., 2006, ApJ, 647, 201
Danovich M., Dekel A., Hahn O., Teyssier R., 2012, MNRAS, 422, 1732
Demers S., Kunkel W.E., 1976, ApJ, 208, 932
Dubinski J., Carlberg R.G., 1991, ApJ, 378, 496
Elahi P.J., Thacker R.J., Widrow L.M., 2011, MNRAS, 418, 320
Elahi P.J., et al., 2013, MNRAS, 433, 1537
Ghez A.M., et al., 2008, ApJ, 689, 1044
Gill S.P.D., Knebe A., Gibson B.K., Dopita M.A., 2004, MNRAS, 351, 410
Goerdt T., Burkert A., 2013, ArXiv e-prints
Hahn O., Teyssier R., Carollo C.M., 2010, MNRAS, 405, 274
Joachimi B., Semboloni E., Bett P.E., Hartlap J., Hilbert S., Hoekstra H., Schneider P., Schrabback T., 2013, MNRAS, 431, 477
Knebe A., Gill S.P.D., Gibson B.K., Lewis G.F., Ibata R.A., Dopita M.A., 2004, ApJ, 603, 7
Knebe A., et al., 2013, MNRAS
Knollmann S.R., Knebe A., 2009, ApJS, 182, 608
Koch A., Grebel E.K., 2006, AJ, 131, 1405
Kravtsov A.V., Gnedin O.Y., Klypin A.A., 2004, ApJ, 609, 482
Libeskind N.I., Frenk C.S., Cole S., Helly J.C., Jenkins A., Navarro J.F., Power C., 2005, MNRAS, 363, 146
Libeskind N.I., Knebe A., Hoffman Y., Gottlöber S., Yepes G., Steinmetz M., 2011, MNRAS, 411, 1525
Libeskind N.I., Hoffman Y., Knebe A., Steinmetz M., Gottlöber S., Metuki O., Yepes G., 2012, MNRAS, 421, L137
Lovell M.R., Eke V.R., Frenk C.S., Jenkins A., 2011, MNRAS, 413, 3013
Lynden-Bell D., 1976, MNRAS, 174, 695
McConnachie A.W., 2012, AJ, 144, 4
Metz M., Kroupa P., Jerjen H., 2007, MNRAS, 374, 1125
Metz M., Kroupa P., Jerjen H., 2009, MNRAS, 394, 2223
Onions J., et al., 2012, MNRAS, 423, 1200
Onions J., et al., 2013, MNRAS, 429, 2739
Pawlowski M.S., Kroupa P., 2013, MNRAS, 435, 2116
Pawlowski M.S., Kroupa P., Angus G., de Boer K.S., Famaey B., Hensler G., 2012, MNRAS, 424, 80
Paz D.J., Lambas D.G., Padilla N., Merchán M., 2006, MNRAS, 366, 1503
Power C., Knebe A., Knollmann S.R., 2012, MNRAS, 419, 1576
Pujol A., et al., 2013, ArXiv e-prints
Reddick R.M., Wechsler R.H., Tinker J.L., Behroozi P.S., 2013, ApJ, 771, 30
Rodríguez-Puebla A., Avila-Reese V., Drory N., 2013, ApJ, 773, 172
Sales L.V., Navarro J.F., Theuns T., Schaye J., White S.D.M., Frenk C.S., Crain R.A., Dalla Vecchia C., 2012, MNRAS, 423, 1544
Simon J.D., Geha M., 2007, ApJ, 670, 313
Skibba R.A., van den Bosch F.C., Yang X., More S., Mo H., Fontanot F., 2011, MNRAS, 410, 417
Smith R.E., Watts P.I.R., 2005, MNRAS, 360, 203
Smith R.E., Watts P.I.R., Sheth R.K., 2006, MNRAS, 365, 214
Springel V., 2005, MNRAS, 364, 1105
Springel V., White S.D.M., Tormen G., Kauffmann G., 2001, MNRAS, 328, 726
Springel V., et al., 2008, MNRAS, 391, 1685
Starkenburg E., et al., 2013, MNRAS, 429, 725
Tormen G., 1997, MNRAS, 290, 411
Trujillo-Gomez S., Klypin A., Primack J., Romanowsky A.J., 2011, ApJ, 742, 16
Vale A., Ostriker J.P., 2004, MNRAS, 353, 189
van Daalen M.P., Angulo R.E., White S.D.M., 2012, MNRAS, 424, 2954
Vera-Ciro C.A., Sales L.V., Helmi A., Frenk C.S., Navarro J.F., Springel V., Vogelsberger M., White S.D.M., 2011, MNRAS, 416, 1377
Wang J., Frenk C.S., Cooper A.P., 2013, MNRAS, 429, 1502
Weilbacher P.M., Duc P.A., Fritze-v. Alvensleben U., 2003, A&A, 397, 545
Weinmann S.M., van den Bosch F.C., Yang X., Mo H.J., 2006, MNRAS, 366, 2
Zentner A.R., Kravtsov A.V., Gnedin O.Y., Klypin A.A., 2005, ApJ, 629, 219
Zhang Y., Yang X., Wang H., Wang L., Mo H.J., van den Bosch F.C., 2013, ApJ, 779, 160
Zolotov A., et al., 2012, ApJ, 761, 71

APPENDIX A: IMPROVED SHAPE MEASUREMENT

To study in detail the bias induced in the shape measurement due to low numbers of tracer points, we perform the following test. We build mock dark matter haloes by generating particle distributions characterised by a given ellipticity and density profile. Using 10000 random realisations of such artificial haloes formed by Ntracers (representing subhaloes or dark matter particles), we measure the mean shape parameters q and s and the corresponding standard deviations for different sets of input shapes as a function of N. The results of this analysis, shown in Fig. A1, reveal that around 1000 tracer particles are required to ensure that the measured shape parameters deviate by less than 10% from the true (input) values. The bias in the shape measurement due to low tracer points is stronger if the shape parameters of the artificial haloes are close to unity, while results are almost unbiased if the shape parameters are below 0.2.

In Fig. A2 we show the measured shape parameters of a mock halo with input $q = 0.9$ and $s = 0.6$ as a function of the number of tracer particles, N. By trial and error we find that the shape measurements $q(N)$ and $s(N)$ can be described with a function of the form

$$q(N) = q_{\rm fit} - \frac{\beta}{1 + N/\gamma}, \qquad \text{(A1)}$$

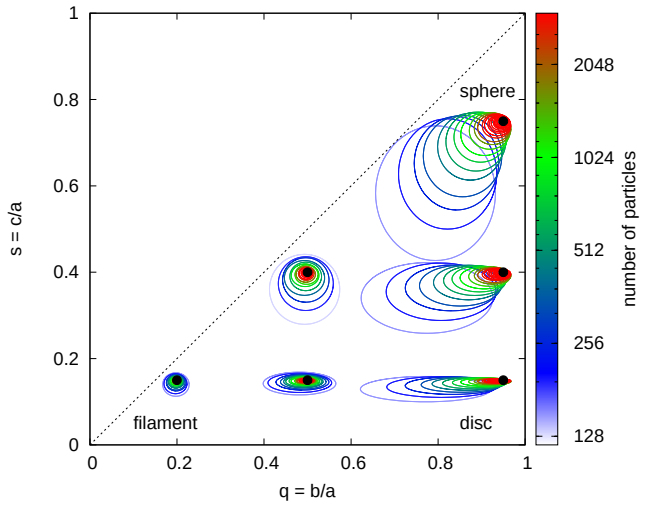

Figure A1. Measured shape parameters of artificial particle distributions with given input shapes, marked by black dots. The centre of the ellipses are the mean measurements of q and s derived from 10000 random realisations of the particle distributions. The major and minor axes denote the standard deviation of q and s measurements, respectively. The colour of the ellipses denotes the number of random particles used in each of the 10000 realisations.

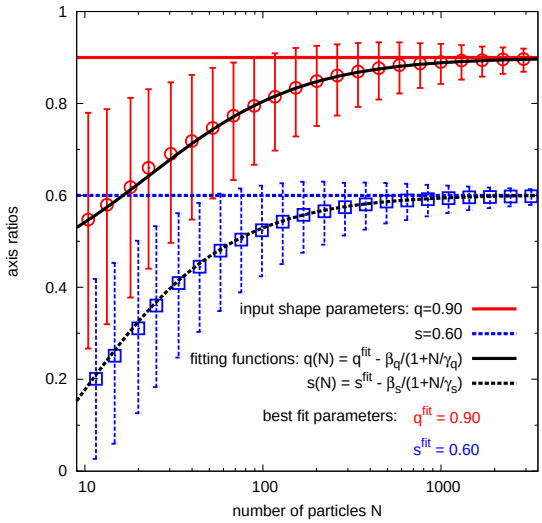
axis ratios
number of particles N
input shape parameters: q=0.90
s=0.60
fitting functions: q(N) = q^fit - β_q/(1+N/γ_q)
s(N) = s^fit - β_s/(1+N/γ_s)
best fit parameters: q^fit = 0.90
s^fit = 0.60

Figure A2. Shape parameters of artificial particle distributions (mimicking a halo with $q = 0.9$ and $s = 0.6$) as a function of the number of tracer particles N. The shape parameters, used to generate the particle distributions, are shown as the coloured horizontal lines. The symbols show the median and central 68% values obtained from 10000 random realisations. Solid and dashed black lines show fits of Eq. A1 to the measurements of q and s, respectively.

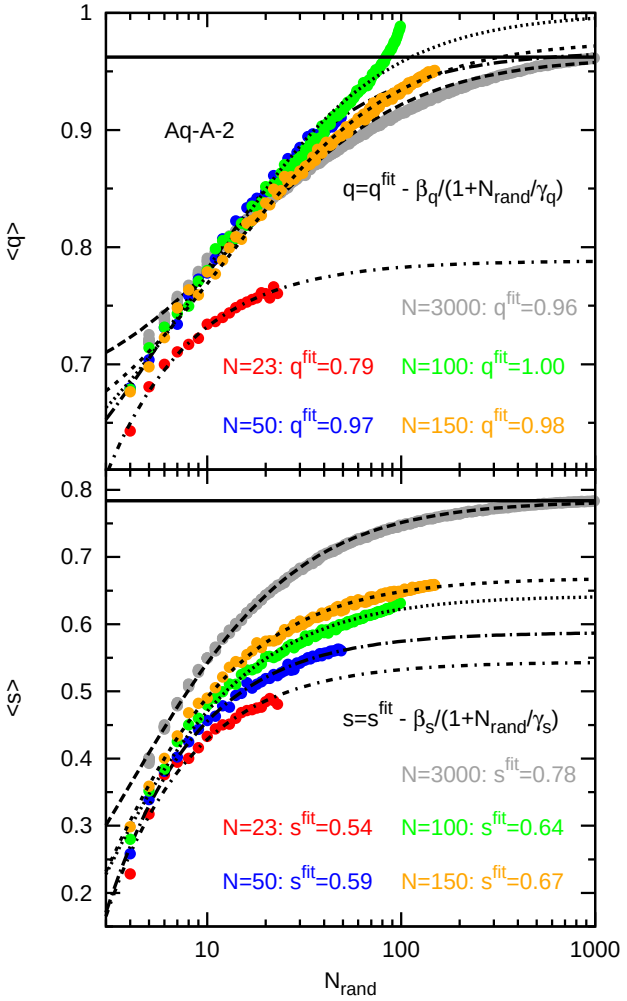

Figure A3. Mean shape parameters derived from 1000 random samples consisting of $N_{\rm rand}$ subhaloes (coloured symbols). The samples are drawn from the N`Aq-A` subhaloes with the highest $v_{\rm max}$ values without replacement. The black dashed lines show the fitting function given by Eq. A1 with the best fit values for $q_{\rm fit}$ and $s_{\rm fit}$ displayed in the figure. The best fit values derived from the $N = 3000$ highest $v_{\rm max}$ subhaloes are shown as black solid lines.

where $q_{\rm fit}$, β and γ are free parameters. The expression for $s(N)$ is analogous to the one for $q(N)$. For large number counts $q(N)$ and $s(N)$ converge, respectively, to $q_{\rm fit}$ and $s_{\rm fit}$, which correspond to the true shape parameters of the halo.

These fitting functions open the possibility to decrease the bias in the shape measurement from low number counts using the following procedure. If we consider the case of the subhalo populations, we randomly sample groups of subhaloes, as much as possible, without replacement. These samples are drawn from the Nhighest $v_{\rm max}$ subhaloes, since in real life only the most massive (or luminous) satellite galaxies are observed. The mean shape parameters of such groups are then measured as a function of the number of group members, $N_{\rm rand}$. By fitting Eq. A1 to the measured $q(N_{\rm rand})$ and $s(N_{\rm rand})$, we can derive the parameters $q_{\rm fit}$ and $s_{\rm fit}$ as shown in Fig. A3.

These fitting parameters tend to lie closer to the shape parameters derived from the 3000 subhaloes with the highest $v_{\rm max}$ values than the shape parameters measured using the $N < 3000$ most massive subhaloes. Indeed, as it is shown in Fig. A4, for the 23 highest $v_{\rm max}$ subhaloes in `Aq-(A-D)`, the difference between $q(N)$ and $q(3000)$ decreases by about

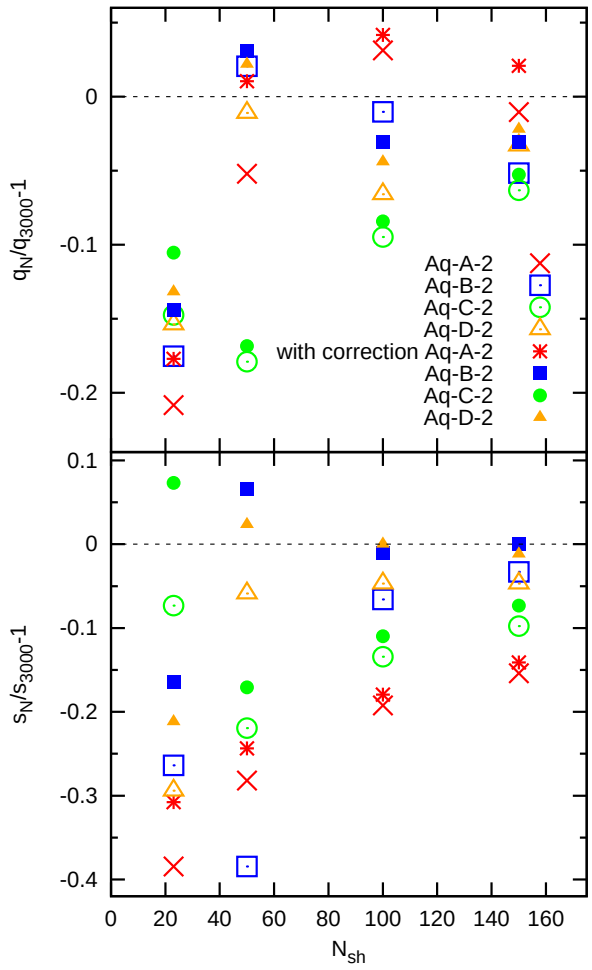

Figure A4. Relative difference between the shape parameters q and s measured from the $N_{\rm sh}$ and 3000 `Aq-(A-D)` subhaloes with the highest $v_{\rm max}$ values. Open symbols show direct q and s measurements, whereas closed symbols represent measurements corrected as described in the text and demonstrated in Fig. A3.

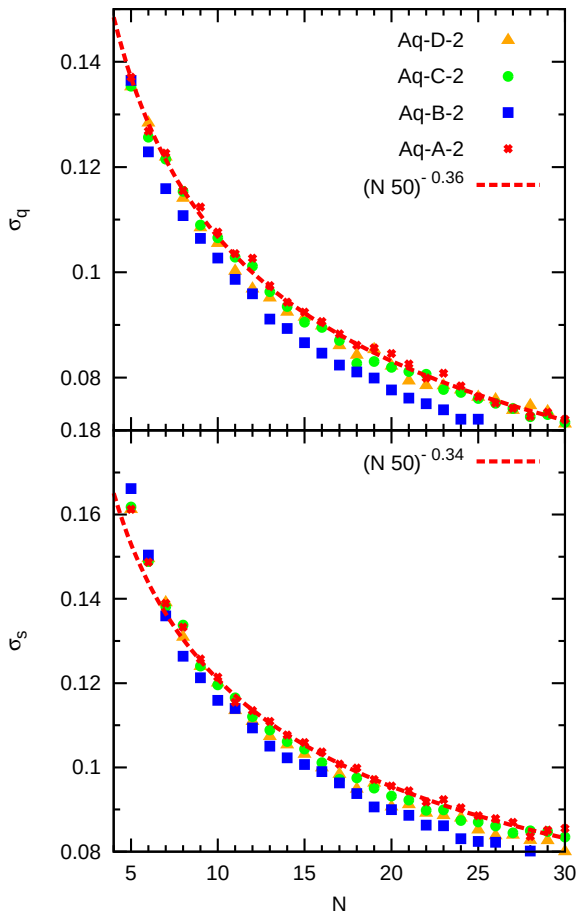

Figure A5. Symbols denote the standard deviation of the shape measurement from randomly selected AHF subhaloes, shown as a blue shaded area in Fig. 2. The red dashed lines are a power law approximation of the `Aq-A` results, used as an error estimation in Fig. 4.

5%, whereas in the case of $s(N)$ the deviation from $s(3000)$ is about 10% smaller if this correction procedure is applied.

APPENDIX B: ERROR ESTIMATIONS FOR THE SHAPE MEASUREMENT

We estimate the error of the shape measurements from the observational data and highest $v_{\rm max}$ `Aq-A` subhaloes shown in Fig. 5 using the results from random sampling Aquarius subhaloes independently of their $v_{\rm max}$ values. The standard deviation derived from sampling NAHF subhaloes 10000 times are shown in Fig. A5. We find that these results can be approximated by a power law shown in the same figure. The error estimate applied to the observational data is the same power law that describes the standard deviation from the `Aq-A` results.

APPENDIX C: MILKY WAY SATELLITES

For comparing the shapes of the Aquarius subhalo distributions to MW data we use the positions and absolute V-band magnitudes of 27 satellite galaxies from McConnachie (2012), presented in Table C1. The distribution of these satellites around the centre of the MW is shown in Fig. C1.

The cartesian coordinates of each satellite are calculated from the heliocentric galactic angles l, b and $r_{\rm GC}$ as follows:

$$x = r_{\rm GC}\cos(b)\cos(l) - d_{\rm GC}$$
$$y = r_{\rm GC}\cos(b)\sin(l)$$
$$z = r_{\rm GC}\sin(b)\,,$$

where the conversion to cartesian coordinates is based on a distance to the galactic centre of $d_{\rm GC} = 8.4\ kpc$ (Ghez et al. 2008). Our cartesian coordinates slightly differ from those given in Pawlowski and Kroupa (2013) due to differences in the angles and in the $d_{\rm GC}$ used for the coordinate conversion. Note that the observational coordinates are given kpc to be consistent with the literature, while we used $h^{-1}kpc$ throughout the paper, since this is the standard output of the GADGET-3 code, which was used for performing the simulations.

Nr.	satellite	l [deg]	b [deg]	$r_\odot$[kpc]	x[kpc]	y[kpc]	z[kpc]	r_{GC}[kpc]	M_V
1	LMC	280.5	-32.9	51	-0.50	-42.10	-27.70	50.40	-18.1
2	SMC	302.8	-44.3	64	16.51	-38.50	-44.70	61.26	-16.8
3	Canis Major	240.0	-0.8	7	-11.80	-6.06	-0.098	13.27	-14.4
4	Sagittarius	5.6	-14.2	26	16.79	2.46	-6.378	18.12	-13.5
5	Fornax	237.1	-65.7	147	-41.16	-50.79	-133.98	149.08	-13.4
6	LeoI	226.0	49.1	254	-123.83	-119.63	191.99	257.88	-12.0
7	Sculptor	287.5	-83.2	86	-5.24	-9.71	-85.40	86.11	-11.1
8	LeoII	220.2	67.2	233	-77.26	-58.28	214.79	235.59	-9.8
9	Sextans	243.5	42.3	86	-36.68	-56.93	57.88	89.08	-9.3
10	Carina	260.1	-22.2	105	-25.01	-95.77	-39.67	106.64	-9.1
11	Draco	86.4	34.7	76	-4.38	62.36	43.27	76.03	-8.8
12	Ursa Minor	105.0	44.8	76	-22.36	52.09	53.55	77.95	-8.8
13	CVn I	74.3	79.8	218	2.15	37.16	214.56	217.76	-8.6
14	Hercules	28.7	36.9	132	84.29	50.69	79.27	126.32	-6.6
15	Bootes I	358.1	69.6	66	14.69	-0.76	61.86	63.59	-6.3
16	LeoIV	265.4	57.4	154	-14.95	-82.70	129.74	154.58	-5.8
17	Bootes III	35.4	75.4	47	1.36	6.86	45.48	46.02	-5.8
18	Ursa Major I	159.43	54.4	97	-61.17	19.84	78.87	101.76	-5.5
19	LeoV	261.9	58.5	178	-21.40	-92.08	151.77	178.80	-5.2
20	PscII	79.2	-47.1	182	14.91	121.70	-133.32	181.13	-5.0
21	CVn II	113.6	82.7	160	-16.44	18.63	158.70	160.64	-4.9
22	Ursa Major II	152.5	37.4	32	-30.85	11.74	19.44	38.30	-4.2
23	Coma Berenices	241.9	83.6	44	-10.61	-4.33	43.73	45.20	-4.1
24	Bootes II	353.7	68.9	42	6.73	-1.66	39.18	39.79	-2.7
25	Wilkman I	158.6	56.8	38	-27.67	7.59	31.80	42.83	-2.7
26	Segue II	149.4	-38.1	35	-32.01	14.02	-21.60	41.08	-2.5
27	Segue I	220.5	50.4	23	-19.45	-9.52	17.72	27.98	-1.5

Table C1. MW satellite galaxies used in this work sorted by the absolute V-band magnitude M_V. This list is based on the table given by McConnachie (2012), where l and b are angles in heliocentric galactic coordinates, $r_\odot$ is the distance to the sun, x, y, z are cartesian coordinates with the centre of the galaxy in the origin, and r_{GC} is the distance to the galactic centre.

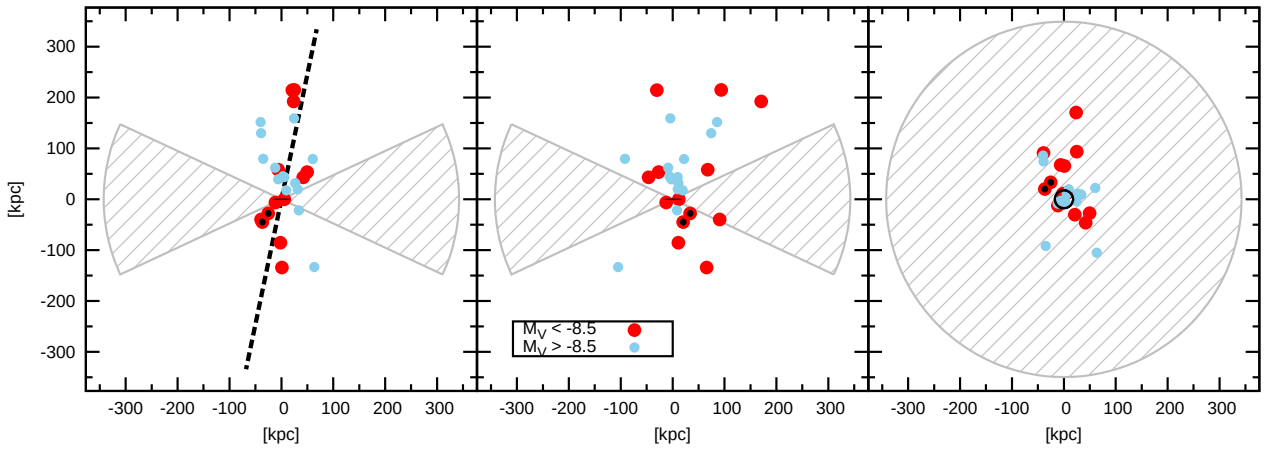

Figure C1. Distribution of satellites from Table C1 around the MW centre. Left and central panel show edge on views on the galactic disc. Coordinates are rotated, so that the best fit plane, spanned by the major and intermediate axis of the ellipsoid fitted to all 27 objects, is edge on in the left panel. The central panel shows the same distribution while the perspective is rotated by 90° around the galactic pole. The right panel shows a face on view on the galactic disc. Red and blue dots denote, respectively, satellites with V-band magnitudes brighter and fainter than $M_V = -8.5$. The shaded area is the assumed galactic obscuration zone used to calculate the shapes for Aquarius subhalo samples shown in the right panel of Fig. 5. Its radial size of 250 $h^{-1}kpc$, with $h = 0.73$ corresponds to the size of the spherical window within which we select Aquarius subhaloes for the analysis. The obscuration angle of 25° is about twice as large as the value usually assumed. Metz et al. (2009) show a similar figure with a smaller galactic obscuration zone together with the projected SDSS light cone, which encloses all faint satellites. The extension of the galactic disc is roughly indicated by black bars in the left and central panel and an open circle in the right panel. Small and large Magellanic Clouds are marked by black dots for orientation.